*Clays and Clay Minerals*, Vol. 61, No. 2, 152–164, 2013.

# ANISOTROPIC SURFACE CHARGING OF CHLORITE SURFACES

XIHUI YIN[1], LUJIE YAN[2], JING LIU[1], ZHENGHE XU[2], AND JAN D. MILLER[1,*]

[1] Department of Metallurgical Engineering, College of Mines and Earth Sciences, University of Utah, 135 South 1460 East, Room 412, Salt Lake City, UT 84112-0114, USA
[2] Department of Chemical and Materials Engineering, University of Alberta, Room 280C, Chemical and Materials Engineering Building, Edmonton, Alberta, AB T6G 2G6, Canada

**Abstract**—Chlorite is a layered silicate mineral group of importance in geology, agriculture, and in the processing of mineral resources. A more detailed analysis of the surface charge of chlorite minerals is important in order to improve our fundamental understanding of such particle structures and their behavior in suspension. In this study, the anisotropic surface charging of chlorite has been established using Atomic Force Microscopy surface-force measurements with a silicon nitride tip. The surface-charge densities and surface potentials at the chlorite basal-plane surfaces and edge surface were obtained by fitting force curves with the Derjaguin-Landau-Verwey-Overbeek theoretical model. The results show that at pH 5.6, 8.0, and 9.0 the chlorite mica-like face is negatively charged with the isoelectric point (IEP) less than pH 5.6. In contrast, the chlorite brucite-like face is positively charged in this pH range and the IEP is greater than pH 9.0. The surface charging of the chlorite edge surface was found to be pH-dependent with the IEP occurring at pH 8.5, which is slightly greater than the edge surfaces of talc and muscovite due to the larger content of magnesium hydroxide at the chlorite edge surface. Findings from the present research are expected to provide a fundamental foundation for the analysis of industrial requirements, *e.g.* collector adsorption, slime coating, and particle interactions in the area of mineral-processing technology.

**Key Words**—Anisotropic Surface Characteristics, Atomic Force Microscopy, Basal Plane, Chlorite, DLVO Model, Edge Surface, Electrophoresis, Flotation, Surface Charge, Surface Potential.

## INTRODUCTION

The group of phyllosilicates, or layered silicates, including serpentine, mica, chlorite, and the clay minerals, is very important in geology, agriculture, and mineral processing (Murray and Kogel, 2005; Harvey and Murray, 1997; Murray, 1991). Some of the phyllosilicates in a pure state are valuable in a wide range of applications including in ceramics, in the manufacture of paper (as a coating, pigment, and filler), in inks and paints (as an extender), in medicine, and as an additive in the production of rubber and polymers (Harvey and Murray, 1997; Murray, 2000). In other circumstances, however, the phyllosilicates, such as kaolinite, illite, and talc, may cause problems in making efficient particle separations in the recovery/utilization of mineral resources and in achieving satisfactory sedimentation/consolidation for disposal of the waste (tailings) from these operations. Note that almost all the aforementioned processes and/or utilization of the phyllosilicates are affected by their crystal structure and surface properties. In this regard, the study of phyllosilicate surface chemistry is critical to the development of improved technology in many sectors of the economy.

The chlorite minerals are a major magnesia silicate group of gangue minerals found in both sulfide and non-sulfide ores. Chlorite is a 2:1:1 type phyllosilicate, consisting of a brucite-like or gibbsite-like sheet sandwiched between mica-like trilayers. The common minerals in the chlorite class include clinochlore ($(Mg_5Al)(AlSi_3)O_{10}(OH)_8$), chamosite ($(Fe_5Al)(AlSi_3)O_{10}(OH)_8$), nimite ($(Ni_5Al)(AlSi_3)O_{10}(OH)_8$), and pennantite ($(Mn, Al)_6(Al, Si)_4O_{10}(OH)_8$). The spacing, the distance between two repeating chlorite layers, is ~1.4 nm. The lattice structure of the brucite-like and mica-like layers of chlorite have been imaged using atomic force microscopy (AFM) (Vrdoljak *et al.*, 1994). When a chlorite crystal is cleaved, both a mica-like face and a brucite-like or gibbsite-like face should be exposed. The mica-like face is expected to carry a permanent negative charge, as 25% of the Si atoms are substituted by Al atoms in the tetrahedral sheet. This charge deficiency is compensated by the positively charged brucite-like or gibbsite-like sheet. Both the negatively charged mica-like layer and the positively charged brucite-like or gibbsite-like sheet contribute to the overall surface-charge density. In addition to the basal plane surfaces, the edge surface of chlorite particles may also have a different charging behavior. The edge surface of phyllosilicates is composed of broken covalent or ionic bonds which have high polarity and are easily hydrolyzed to exhibit a strong pH-dependent surface-charge density (Nalaskowski *et al.*, 2007; Fuerstenau and Pradip, 2005).

Electrophoresis is a common method for determining the zeta potential which represents the electrostatic

* E-mail address of corresponding author:
Jan.Miller@utah.edu
DOI: 10.1346/CCMN.2013.0610212

potential close to the surface at the slipping plane when the particles are moving in the aqueous solution under the influence of an electric field. The pH at which the slipping plane carries zero net charge is known as the isoelectric point (IEP). The zeta potential of chlorite has been studied by several researchers using the electrophoresis technique (Sondi and Pravdic, 1996; Sondi *et al.*, 1996, 1997; Fornasiero and Ralston, 2005). The measured IEP is in the range of pH 3 to 6, depending on different mineralogy and electrolyte conditions. Note that the zeta potential calculated from electrophoretic measurements assumes that the particles are spherical and does not take into account the platy shape and anisotropic character of phyllosilicate particles.

Mular-Roberts titration is another technique used to characterize the surface charging. In this method, the pH value of a suspension is measured at different ionic strengths. The suspension is first prepared at given pH and ionic strength; then the ionic strength is increased to yield a change in pH (Mular and Roberts, 1966). When no change in pH occurs, the pH value is determined as the point of zero salt effect (PZSE). Using the Mular-Roberts titration technique, Alvarez-Silva *et al.* (2010) determined the PZSE of chlorite as pH 4.7, compared to an electrophoretic IEP at pH < 3. Some researchers consider the titration method to be a better technique as it is not affected by the particle shape. Like the electrophoresis technique, however, the titration technique still only gives an overall surface charge density and the anisotropic surface charging characteristics of phyllosilicate particles are not defined.

Atomic force microscopy has been applied widely in the investigation of the surface properties for different minerals (Veeramasuneni *et al.*, 1996; Nalaskowski *et al.*, 2007; Assemi *et al.*, 2006; Zhao *et al.*, 2008; Yan *et al.*, 2011; Yin and Drelich, 2008; Long *et al.*, 2009; Gupta *et al.*, 2011). According to the geometry of the AFM tips, several theoretical models have been developed based on the Derjaguin-Landau-Verwey-Overbeek (DLVO) theory in which the electrostatic interaction and van der Waals interaction are considered. A common technique used for surface-force measurements is known as the colloidal probe technique in which a small particle with spherical shape is glued at the end of a tipless AFM cantilever (Nalaskowski *et al.*, 2003; Wallqvist *et al.*, 2006; Zhang *et al.*, 2007). The colloidal probe technique can greatly enhance the sensitivity of surface-force measurements. However, the spherical particles used in the measurements are usually 5−20 μm in size. Thus, obtaining a high-resolution image during the surface-force measurements is difficult. The roughness of the particle surfaces may also influence significantly the surface forces.

By using the colloidal probe technique, the surface charging property can be determined. Generally, AFM measures the diffuse-layer potential or diffuse-layer charge. The IEP is often used to describe a surface electrostatic potential of zero from AFM measurements. Although the values of IEP determined by AFM and electrophoretic mobility may not be exactly the same, they are usually very close to each other (Leroy *et al.*, 2011; Drelich and Wang, 2011). The surface-charging behaviors of the talc basal-plane surface and the edge surface were found by Nalaskowski *et al.* (2007) to be different. However, the surface roughness of their samples was still too great to acquire reliable AFM force curves and perform a detailed quantitative analysis. In another study (Zhao *et al.*, 2008), the quality of the edge surfaces was improved using a microtome cutting technique to create a smooth surface. Subsequently, the interaction forces between a silica probe particle and muscovite face and edge surfaces were measured by Zhao *et al.* (2008). Ultra-smooth (roughness <1 nm) mica and talc basal-plane and edge surfaces were prepared successfully by Yan *et al.* (2011). The anisotropic surface-charging characteristics for mica and talc basal-plane surfaces and edge surfaces have been characterized using AFM.

The present study discusses the surface charging of chlorite as a function of pH measured by electrophoresis and AFM. The IEPs for the chlorite mica-like face, brucite-like face, and edge surfaces were determined from surface force measurements using AFM. In this way, the anisotropic charging properties for chlorite were established. The present research is expected to provide a better understanding of the anisotropic surface-chemistry properties of chlorite which is significant for developing suitable flotation reagent schedules (collectors, depressant, modifiers, and pH) and improving flotation separation processes.

## MATERIALS AND METHODS

### *Sample preparation*

A high-purity chlorite crystal with natural cleavage on the (001) plane from Chester, Pennsylvania, USA, was used. X-ray diffraction (XRD) results implied that the chlorite sample is highly ordered and the basal reflections (001), (002), (003), (004), (005) of chlorite were observed. No other possible mineral contaminants were detected in the XRD pattern. X-ray photoelectron spectroscopy (XPS) analysis showed that the chlorite sample contains 7.5% Si, 4.9% Al, 9.9% Mg, and trace amounts of Na (0.2%), Fe (0.3%), Cr (0.7%), and chloride (0.2%). The XPS results suggested that the chlorite sample being studied corresponded most closely to clinochlore. A few flakes of chlorite sample were ground to <45 μm in size to measure the zeta potential using the electrophoresis method.

One thin layer of chlorite was peeled from the chlorite crystal using sticky tape. This thin layer of the chlorite crystal as well as the chlorite crystal itself were then glued on two thoroughly cleaned glass substrates. As chlorite is composed of alternating mica-like layers and brucite-like sheet structures, when a chlorite sample

https://doi.org/10.1346/CCMN.2013.0610212 Published online by Cambridge University Press

is cleaved, two different faces will be exposed. By using this method, chlorite samples exposing a mica-like surface and a brucite-like surface were prepared (Figure 1). Note that the cleavage of chlorite can be random. Thus, either a mica-like layer or brucite-like sheet can be exposed at the top of the tape. After keeping the sample in a petri-dish for 24 h until the glue was completely dry, the samples were mounted on magnetic disks as the substrate for study of the charging properties of chlorite surfaces using AFM. Before measuring the surface force by AFM, the samples were dried and cleaned with high-purity nitrogen gas to remove any contaminants.

The chlorite edge surface was also prepared. A small flake of the chlorite sample was embedded in epoxy resin (Electron Microscopy Sciences, Hatfield, Pennsylvania, USA) and baked for 24 h at 60ºC. Then the sample was trimmed using a razor blade under an optical microscope to make the sample perpendicular to the cutting edge. When the chlorite edge was exposed, the sample was glued on a magnetic disk and cut using an ultramicrotome (EM UC 7, Leica Microsystems, Inc.) to obtain a smooth surface for subsequent AFM study. Before measuring the surface force by AFM, the samples were rinsed with Milli-Q water and ethanol and cleaned with high-purity nitrogen gas to remove any debris or contaminants.

*Zeta-potential measurements*

The zeta-potential measurements were done using the electrophoresis technique (ZetaPALS, Brookhaven Instrument Corp., New York). A chlorite suspension with a concentration of 0.05 wt.% was prepared in 1 mM KCl background electrolyte. The mobilities of chlorite particles were measured at varying pH and then converted to zeta potentials (ζ) using Smoluchowski's model as follows:

$$U = \frac{\varepsilon\zeta}{4\pi\eta} E_{\infty} \quad (1)$$

where $U$ is the particle mobility, $E_{\infty}$ is the strength of the electric field applied, and ε and η are the dielectric constant and viscosity of the solvent, respectively. The Smoluchowski model assumes that the particles are spherical and that the surface-charge densities are uniformly distributed at the particle surfaces.

*Surface-force measurements using AFM*

A picoforce AFM with a Nanoscope V controller (Bruker Corporation, Santa Barbara, California, USA) was used with a PF-type scanner designed for picoforce measurements. A contact-mode silicon nitride cantilever was used to study the surface charging of chlorite. The spring constant was determined by the thermal tuning function provided in *Nanoscope V* 7.20 software and this value was used later in data analysis. The AFM images of chlorite basal planes and edge surfaces were collected before the surface force measurements were taken. The images were captured with a scan size of 5 μm and scan rate of 1 Hz. The resolution of the image is 512 points/line.

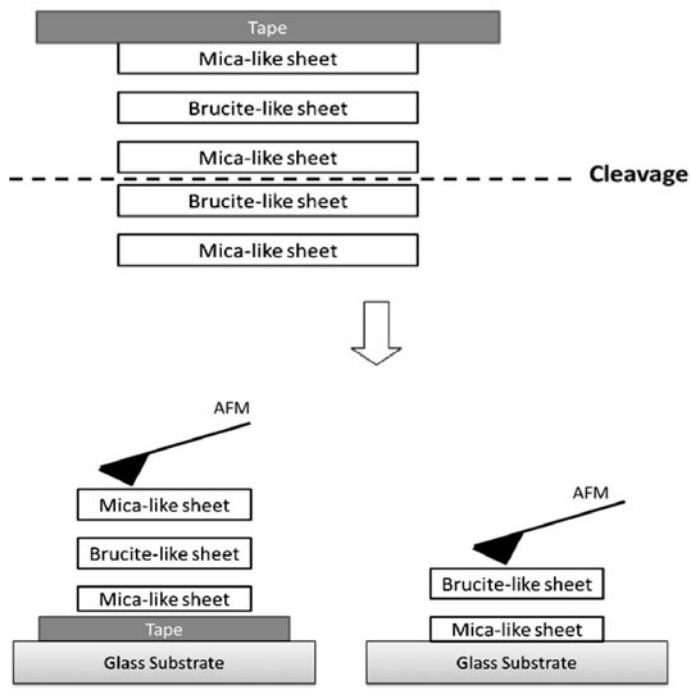


Figure 1. Schematic diagram of the preparation procedure for chlorite basal surfaces.

https://doi.org/10.1346/CCMN.2013.0610212 Published online by Cambridge University Press

The surface-force measurements were conducted at the chlorite mica-like surface, the brucite-like surface, and the edge surface at five different locations in 1 mM KCl at pH 5.6, 8, and 9. At each location, five force curves were collected. All the force measurements were performed at a scan rate of 1 Hz and captured at a resolution of 512 points/measurement. *SPIP* software (Image Metrology, Lyngby, Denmark) was used to convert the deflection-distance curves to force-distance curves. Baseline correction and hysteresis correction were involved in preparation of the force curves. The force-distance curves were fitted with the theoretical DLVO model under constant surface-charge density or a constant surface-potential boundary condition. The surface charge density and the surface potential of various types of clay surfaces were obtained from fitting the force profile data to the DLVO theory.

*Theoretical model*

The geometry of the silicon nitride AFM tip can be approximated as being conical in shape with a spherical cap at its apex. The geometry of the system and the parameters used are shown in Figure 2. The symbols α and β are the geometrical angles for the spherical cap at the tip end and conical tip with α+β = 90º, $D$ is the distance from the end of the tip to the substrate, $L$ is the distance between a differential surface section of the tip and the substrate, $r$ is the radius of the circle of the tip at a given vertical position, and $R$ is the radius of the spherical cap at the tip end (Drelich *et al.*, 2007).

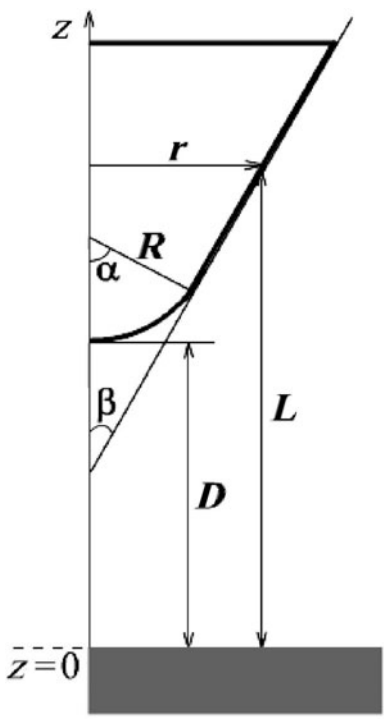


Figure 2. Geometry of the system and parameters used for theoretical DLVO calculations.

The DLVO theoretical model with this geometry was derived and discussed in the literature (Drelich *et al.*, 2007) and only the final equations are given here.

The van der Waals force between the spherical segment of the tip and flat substrate surface is given by:

$$F_{TS}^{vdw\text{-}S} = \frac{A}{6}\left[\frac{(R+D)-2L_1}{L_1^2} - \frac{R-D}{D^2}\right] \quad (2)$$

The formula describing the van der Waals force for the conical segment of the AFM tip is:

$$F_{TS}^{vdw\text{-}C} = \frac{A}{3\tan^2\alpha}\left(\frac{1.0}{L_1} + \frac{R\sin\alpha\tan\alpha - D - R(1-\cos\alpha)}{L_1^2}\right) \quad (3)$$

where $L_1 = D+R(1-\cos\alpha)$, A is the combined Hamaker constant, ε is the dielectric constant of the solution in this system, $\varepsilon_0$ is the permittivity of vacuum, $1/\kappa$ is the Debye length, $D$ is the distance between the two surfaces, and subscripts 1 and 2 refer to the two surfaces. ($A_{water} = 3.7\times10^{-20}$ J, $A_{tip} = 1.62\times10^{-19}$ J, $A_{chlorite} = 2.33\times10^{-19}$ J (Isrealachvili, 1985; Vincent and Jean Marc, 2007)).

The electrostatic forces with constant surface potential for the spherical part and the conical part of the tip are given by:

$$F_{TS}^{S} = 4\pi\varepsilon_0\varepsilon\Phi_T\Phi_S(a_0e^{-\kappa D} - a_1^{-\kappa L_1}) - 2\pi\varepsilon_0\varepsilon(\Phi_T^2+\Phi_S^2)(a_1e^{-2\kappa D} - a_3^{-2\kappa L_1}) \quad (4)$$

where $\Phi_T$ and Φs are the surface potentials of AFM tip and surface, $a_0 = \kappa R-1$, $a_1 = \kappa R\cos\alpha-1$, $a_2 = a_0+0.5$, and $a_3 = a_1+0.5$.

$$F_{TS}^{C} = \frac{4\pi\varepsilon_0\varepsilon\kappa}{\tan\alpha}\left[b_1\Phi_T\Phi_Se^{\kappa L_1} - b_2\frac{(\Phi_T^2+\Phi_S^2)}{2}e^{2\kappa L_1}\right] \quad (5)$$

The electrostatic force with constant surface charge density for the spherical part and the conical part of the tip is given by:

$$F_{TS}^{S} = \frac{4\pi}{\varepsilon_0\varepsilon\kappa^2}\sigma_T\sigma_S(a_0e^{-\kappa D} - a_1e^{-\kappa L_1}) + \frac{2\pi}{\varepsilon_0\varepsilon\kappa^2}(\sigma_T^2+\sigma_S^2)(a_2e^{-2\kappa D} - a_3e^{-2\kappa L_1}) \quad (6)$$

$$F_{TS}^{C} = \frac{4\pi}{\varepsilon_0\varepsilon\kappa\tan\alpha}\left[b_1\sigma_T\sigma_Se^{-\kappa L_1} + b_2\frac{(\sigma_T^2+\sigma_S^2)}{2}e^{-2\kappa L_1}\right] \quad (7)$$

where $\sigma_T$ and $\sigma_s$ are the surface charge densities of AFM tip and surface, respectively,

$$b_1 = \left[R\sin\alpha - \frac{D+R(1-\cos\alpha)}{\tan\alpha}\right] + \frac{1}{\tan\alpha}\left[\left(L_1+\frac{1}{\kappa}\right)\right] \quad (8)$$

https://doi.org/10.1346/CCMN.2013.0610212 Published online by Cambridge University Press

$$b_2 = \left[R\sin\alpha - \frac{D + R(1-\cos\alpha)}{\tan\alpha}\right] + \frac{1}{\tan\alpha}\left[\left(L_2 + \frac{1}{2\kappa}\right)\right] \quad (9)$$

The total electrostatic force between the tip and the substrate can then be obtained for either constant surface potential or constant surface charge density by the sum of these two parts:

$$F^{e} = F^{S}_{TS} + F^{C}_{TS} \quad (10)$$

The total DLVO force for the system with geometry shown in Figure 2 is given by adding the electrostatic force and the van der Waals force:

$$F = F^{e} + F^{vdw} \quad (11)$$

The surface potential is calculated from the surface-charge density using the Grahame equation (Isrealachvili, 1985) which is expressed as

$$c_0 = c_\infty \exp\left(-\frac{z_i e\Psi}{kT}\right) \quad (12)$$

$$c_0 - c_\infty = \frac{\sigma^2}{2\varepsilon\varepsilon_0 kT} \quad (13)$$

$$c_\infty = \frac{\kappa\varepsilon\varepsilon_0 kT}{e^2 z^2} \quad (14)$$

where $\Psi$ is the surface potential, k is the Boltzmann constant, $T$ is the absolute temperature, $e$ is the electronic charge, $z$ is the valence of the ions, $c_0$ is the ionic concentration at the surface, and $c_\infty$ is the ionic concentration in the bulk at $x = \infty$ where $\Psi(\infty) = 0$.

## RESULTS AND DISCUSSION

### *Zeta potential of chlorite measured by electrophoresis*

The results of the zeta potentials of chlorite particles determined by electrophoresis (Figure 3) indicate that the IEP of chlorite is ~pH 5.5, a result which is in good agreement with the value given by Fornasiero and Ralston (2005). According to the crystalline structure of chlorite, both a mica-like face and a brucite-like face can be exposed at a particle surface and contribute to the surface-charge density of chlorite. Usually, mica-group minerals have an IEP of <pH 2, whereas brucite has a larger IEP which is ~pH 11 (Pokrovsky and Schott, 2004; Fuerstenau *et al.*, 2007). The IEP measured for chlorite in the present study is close to the average value of the IEP for mica and brucite. Note, however, that the IEP determined from electrophoretic mobility may be misleading due to the basic assumption in the Smoluchowski model that the particles are of spherical shape (Butt *et al.*, 2003) and of homogeneous surface-charge density (Nalaskowski *et al.*, 2007; Wypych and Satyanarayana, 2004). Chlorite is known to be a mineral with platy morphology and anisotropic surface characteristics. The surface charge at the two basal planes (mica-like face and brucite-like face) and at the edge surface can be different. Therefore, the zeta potential obtained from electrophoresis with the Smoluchowski model may not reflect the surface potential at the shear plane. So far, no model is available to describe the

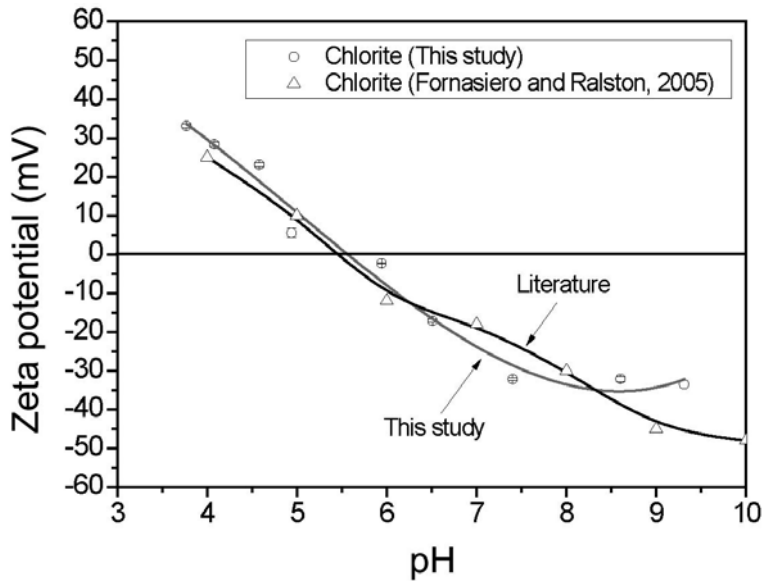


Figure 3. Zeta potential of chlorite as a function of pH measured in 1 mM KCl by the electrophoresis method compared with the results reported in the literature (Fornasiero and Ralston, 2005). The error bars denote the standard deviation of multiple surface force measurements.

https://doi.org/10.1346/CCMN.2013.0610212 Published online by Cambridge University Press

movement of platy-shaped particles with anisotropic surface-charging characteristics. Hence, the anisotropic surface charge of chlorite needs to be characterized using other techniques.

*Interaction forces at chlorite basal-plane surfaces*

Surface forces were measured at both the chlorite mica-like face surface and the brucite-like surface. The chlorite basal plane surface (Figure 4a) was determined to be the mica-like face by subsequent AFM surface-force measurements. The root-mean-square surface roughness for the chlorite basal-plane surface was determined to be from 0.1 to 0.4 nm. This roughness suggests that the chlorite basal-plane surfaces are smooth enough to satisfy the requirements of AFM surface force measurement.

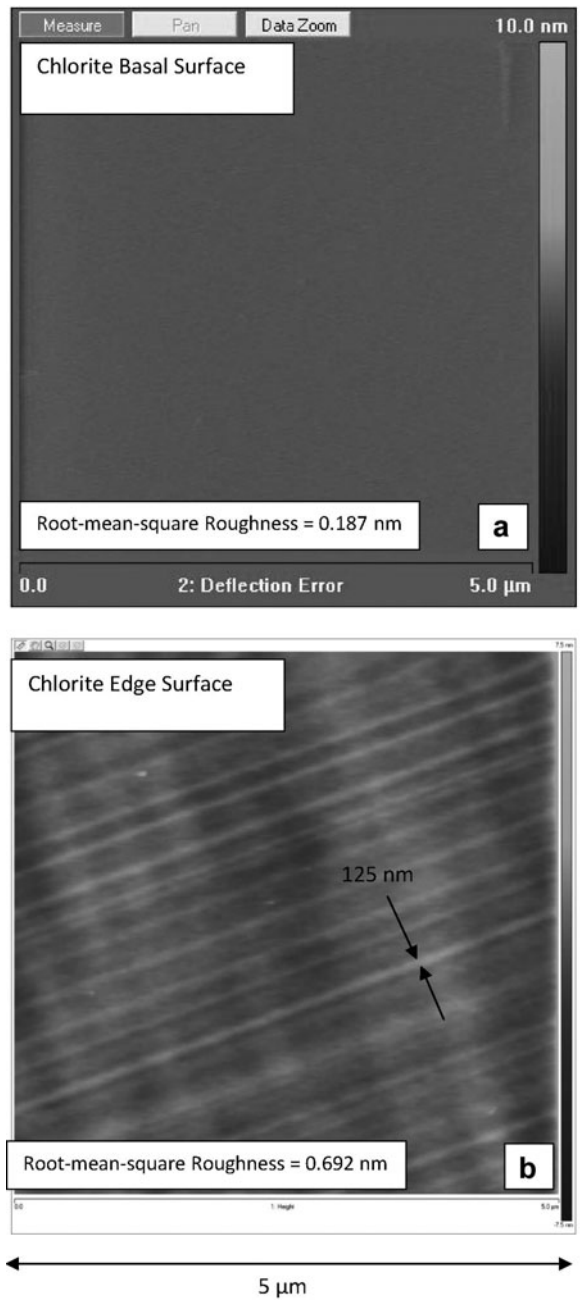


Figure 4. Typical AFM image of chlorite mica-like basal plane surface (a) and edge surface (b).

The approaching surface-force curves were collected at both types of basal planes of chlorite. The typical interaction forces between the silicon nitride AFM tip and the chlorite mica-like surface in 1 mM KCl solutions with varying pH values are shown in Figure 5. A 10−20% variation on the magnitude of the surface forces was observed during the AFM surface-force measurements. The open circles on the graphs represent experimental data, whereas the solid lines represent data calculated using the DLVO theoretical model. For the curve fitting, the surface-charge densities of the silicon nitride AFM tip at different pH values were taken from the literature (Yan *et al.*, 2011). The IEP of the silicon nitride AFM tip is noted to be ~pH 4.0 (Yin and Drelich, 2008). Thus, the tip should be negatively charged at pH 5.6, 8.0, and 9.0. The experimental surface-force curves are in good agreement with the curves calculated from the theoretical model at separation distance >5 nm (Figure 5). However, at shorter separations, the theoretical fitting curves deviated from the experimental curves. The strong repulsive interactions recorded at separations below 1−2 nm might be attributed to a non-DLVO force known as the 'hydration force' which was not taken into account in the theoretical model used in the present study. Electrostatic interaction is usually observed at separation distances of 5 to 30 nm. Long-range repulsive forces were observed at all three pH conditions (Figure 5). The magnitude of the repulsion increased gradually with an increase in pH. The results indicate that chlorite mica-like face is negatively charged in this pH range and the IEP of the chlorite mica-like face is <pH 5.6.

In contrast to the mica-like face of chlorite, attractive interactions dominate the brucite-like face of chlorite at all three pH values (5.6, 8.0, and 9.0), suggesting that it is positively charged in this pH range and its IEP should be >pH 9 (Figure 6).

## INTERACTION FORCES AT CHLORITE EDGE SURFACES

A representative AFM image of the chlorite edge surface is shown in Figure 4b. The root-mean-square surface roughness was determined to be 0.692 nm, confirming that the ultramicrotome cutting technique is capable of creating a 'molecularly smooth' flat surface which can be used for AFM surface-force measurements. The pattern of lines arises from the chlorite sheets (Figure 4b). The distances between the lines were measured as 80−130 nm. Compared to the distances

https://doi.org/10.1346/CCMN.2013.0610212 Published online by Cambridge University Press

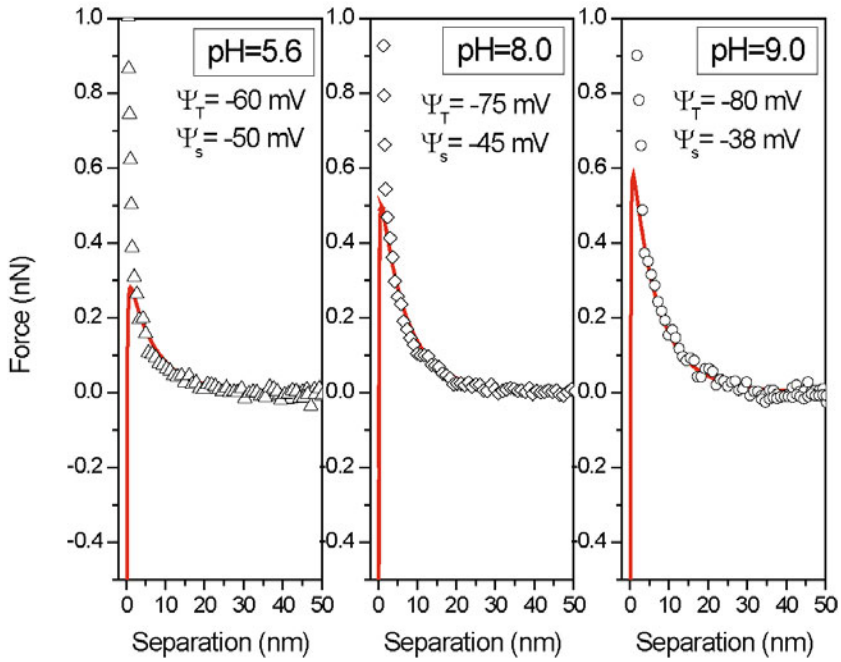


Figure 5. Interaction forces between a silicon nitride AFM tip and chlorite mica-like basal plane surface in 1 mM KCl at pH 5.6, 8.0, and 9.0. The solid lines represent the theoretical DLVO fit. $\Psi_T$ is the surface potential of the silicon nitride AFM tip and $\Psi_S$ is the surface potential of the chlorite mica-like surface.

between repeating chlorite units, which is ~1.4 nm, the results suggest that there are ~60 to 90 repeating units between two lines.

The surface-force measurements were performed at the well prepared chlorite edge surface using AFM. Representative surface-force curves between the silicon

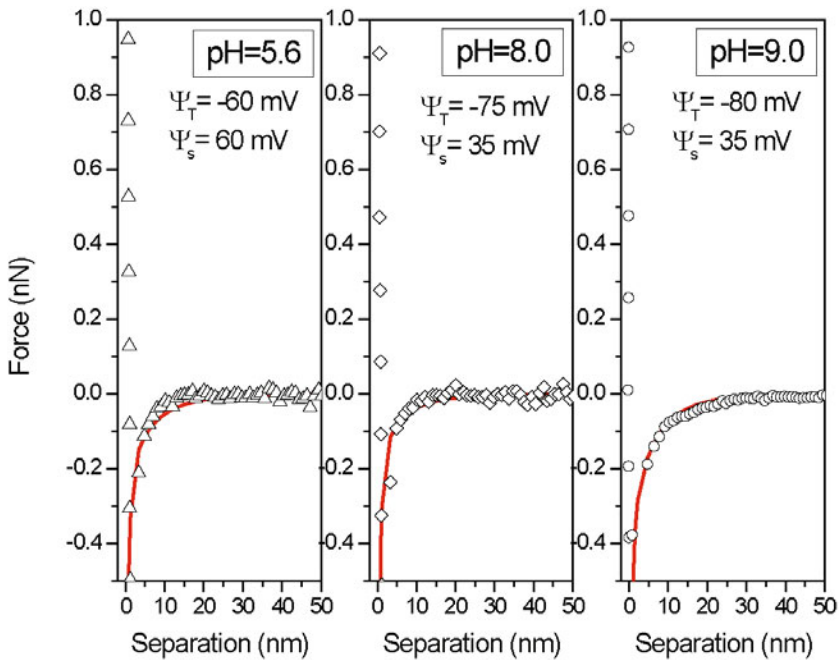


Figure 6. Interaction forces between a silicon nitride AFM tip and chlorite brucite-like basal plane surface in 1 mM KCl at pH 5.6, 8.0, and 9.0. The solid lines represent the theoretical DLVO fit. $\Psi_T$ is the surface potential of the silicon nitride AFM tip and $\Psi_S$ is the surface potential of the chlorite brucite-like surface.

https://doi.org/10.1346/CCMN.2013.0610212 Published online by Cambridge University Press

nitride AFM tip and chlorite edge surface were acquired in 1 mM KCl with varying pH values (Figure 7).

The experimental data were fitted with the theoretical DLVO model and good agreement was observed. Though the DLVO model applies to a planar surface of infinite extent with uniform point charges, few substrates satisfy this condition. The fact that a nano-sized probe was used, which was smaller than the width of edges, should justify this approximation. This condition is not perfect as the tip is slightly smaller than the width of the edge but as a first approximation is acceptable. At pH 5.6 and 8.0, attractive interaction forces were found between the AFM tip and chlorite edge surface. When the pH value of the electrolyte was increased to pH 9.0, the interaction force became repulsive. As the silicon nitride AFM tip is negatively charged at all three pH conditions, these surface force results suggest that the chlorite edge surface is pH dependent. The chlorite edge surface is positively charged below pH 8.0 and negatively charged above 9.0, indicating that the IEP of the chlorite edge lies between pH 8.0 and pH 9.0.

*Surface potential and surface-charge density*

The magnitudes of surface-charge density and surface potential of the chlorite mica-like surface and brucite-like surface (Figure 8) were determined from fitting the experimental force curves to the DLVO model. At pH 5.6, 8.0, and 9.0, the mica-like face of chlorite is negatively charged, with the surface potential between −45 mV and −50 mV and the surface charge density between −5.8 mC/m$^2$ and −6.6 mC/m$^2$. The surface potential of the chlorite mica-like face was noted to be nearly constant over the pH range which confirms that the pH-insensitive surface-charge density is attributed to the presence of a permanent and fixed amount of isomorphous substitution of $Si^{4+}$ by $Al^{3+}$ in the chlorite mica-like face. The silica tetrahedral face, which has a hexagonal ring structure, is known to be difficult to protonate (Avena *et al.*, 2003). The charge deficiency caused by lattice substitution is, therefore, believed to account for the permanent negative charge on this basal plane. The results from characterization of the surface charging of muscovite and talc basal planes using AFM (Yan *et al.*, 2011) are compared in Figure 8b. Similar to the chlorite mica-like face, the basal planes for talc and muscovite are also negatively charged and the surface potentials are nearly constant. These results confirm the pH-insensitive nature of the silica tetrahedral face for phyllosilicate minerals. Note that the magnitude of the surface potentials for the basal planes of these three phyllosilicates are in a sequence of $\Psi$(talc) < $\Psi$(chlorite mica-like) < $\Psi$(muscovite), which may be due to the different levels of isomorphous substitution. In a perfect muscovite lattice, the isomorphous substitution should be 25%. In contrast, talc has a much smaller amount of isomorphous substitution (0.01−3.4%), which results in a smaller surface potential (Deer *et al.*, 1997). In the case of chlorite, $Al^{3+}$ could be present in both the mica-like face and in the brucite-like face by isomorphous substitution. Thus, the level of substitution in the mica-

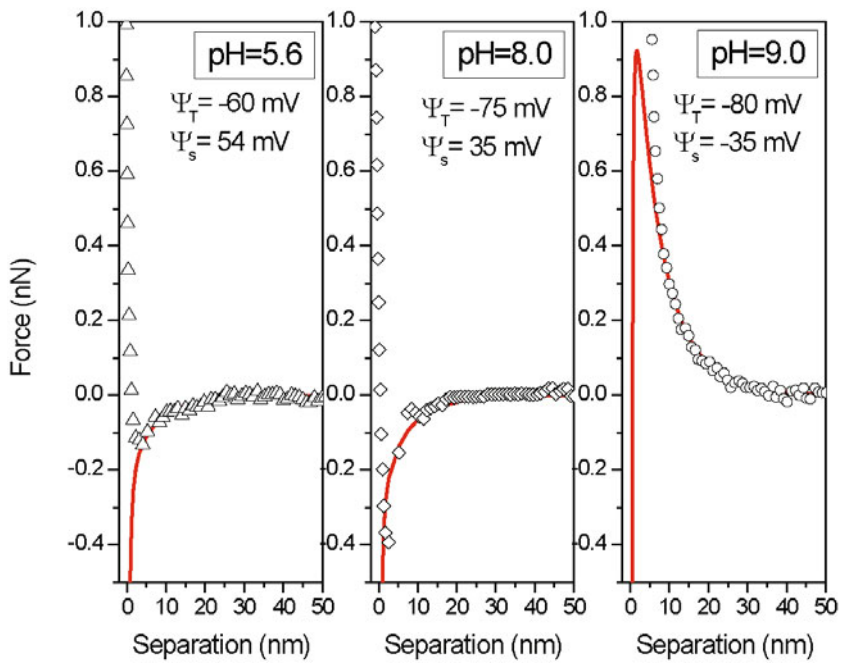


Figure 7. Interaction forces between a silicon nitride AFM tip and chlorite edge surface in 1 mM KCl at pH 5.6, 8.0, and 9.0. The solid lines represent the theoretical DLVO fit. $\Psi_T$ is the surface potential of the silicon nitride AFM tip and $\Psi_S$ is the surface potential of the chlorite edge surface.

https://doi.org/10.1346/CCMN.2013.0610212 Published online by Cambridge University Press

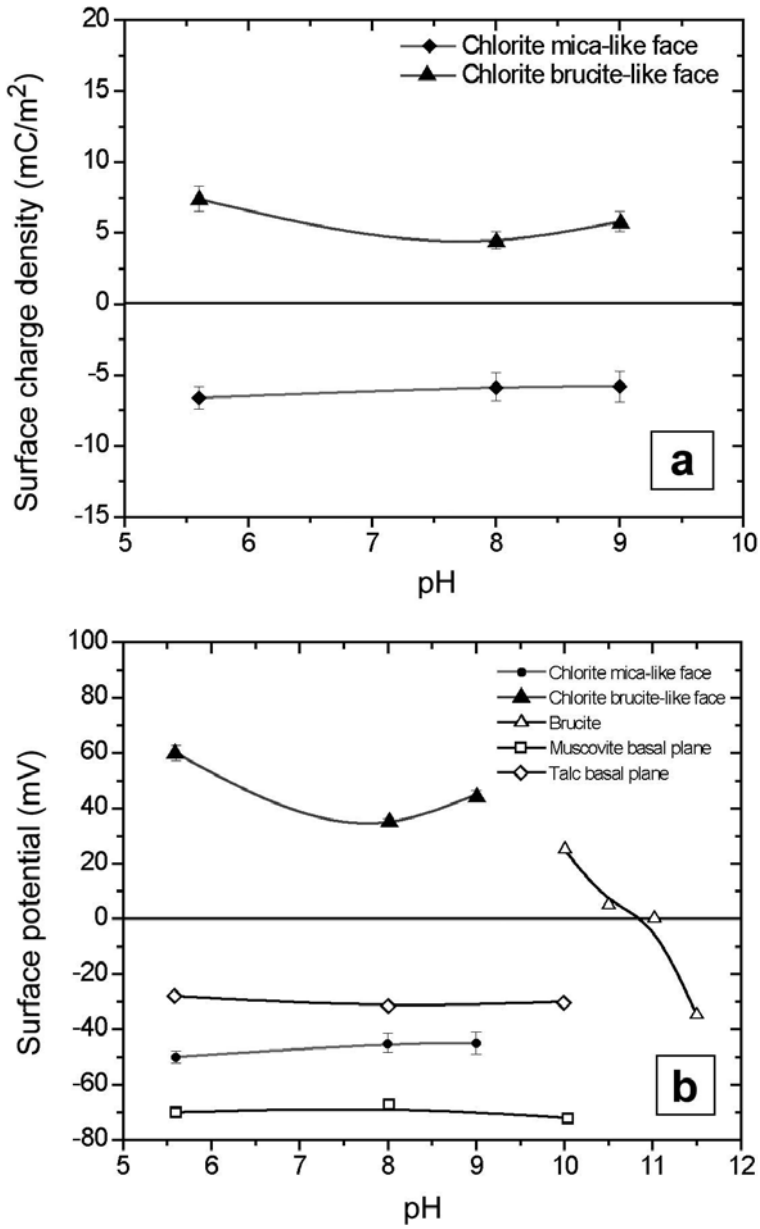


Figure 8. Surface charge density (a) and surface potential (b) of the chlorite mica-like basal plane surface and brucite-like basal plane surface as a function of pH. The error bars denote the standard deviation of multiple surface force measurements. The surface potentials of chlorite basal planes (Solid symbols) are compared with the literature results (plot with open symbols) (Pokrovsky and Schott, 2004; Yan *et al.*, 2011).

like face is difficult to estimate. Moreover, from the elemental composition analysis, note that other cations including $Fe^{2+}$, $Cr^{2+}$, and $Na^{+}$ are also involved in the chlorite lattice. These cations will also affect the magnitude of the surface potential.

The surface-charge densities and surface potentials of the chlorite brucite-like face are also plotted in Figure 8. At all three pH values, the brucite-like face of chlorite is positively charged. The surface potentials are in a range of 35 to 60 mV and the surface-charge densities are between 4.5 and 7.5 mC/m$^2$. A slight decrease in surface potential with increasing pH was observed, suggesting that the brucite-like face of chlorite is slightly pH-dependent. This finding suggests that, compared with mica-like basal planes, the brucite-like basal planes are less resistant to hydrolysis, leading to pH-dependent ionization of hydrolyzed surface magnesium ions. In order to compare the surface charging behavior of chlorite brucite-like face and brucite, the surface potential of brucite particles from electrophoresis

https://doi.org/10.1346/CCMN.2013.0610212 Published online by Cambridge University Press

measurements reported by Pokrovsky and Schott (2004) are also shown in Figure 8b. Below pH 11.0, the brucite particles are positively charged, which is similar to the chlorite brucite-like face. Nevertheless, as mentioned previously, the $Al^{3+}$ cations are also present in the chlorite brucite-like sheet. Thus, the IEP of the chlorite brucite-like face could be <pH 11.0.

The surface-charge density and surface potential of the chlorite edge surface were measured in 1 mM KCl at pH 5.6, 8.0, and 9.0 (Figure 9). At pH 5.6 and pH 8.0, the surface potentials of the chlorite edge surface are positive with magnitudes of 54 and 35 mV, respectively. When increasing the pH value to pH 9.0, the surface potential is reversed to negative and the surface potential is −35 mV. These results suggest that the chlorite edge surface is strongly pH-dependent and the IEP is estimated to be ~pH 8.5.

The surface potentials of the chlorite edge surface are compared with the surface potential values of muscovite and talc edge surfaces from the literature (Yan *et al.*,

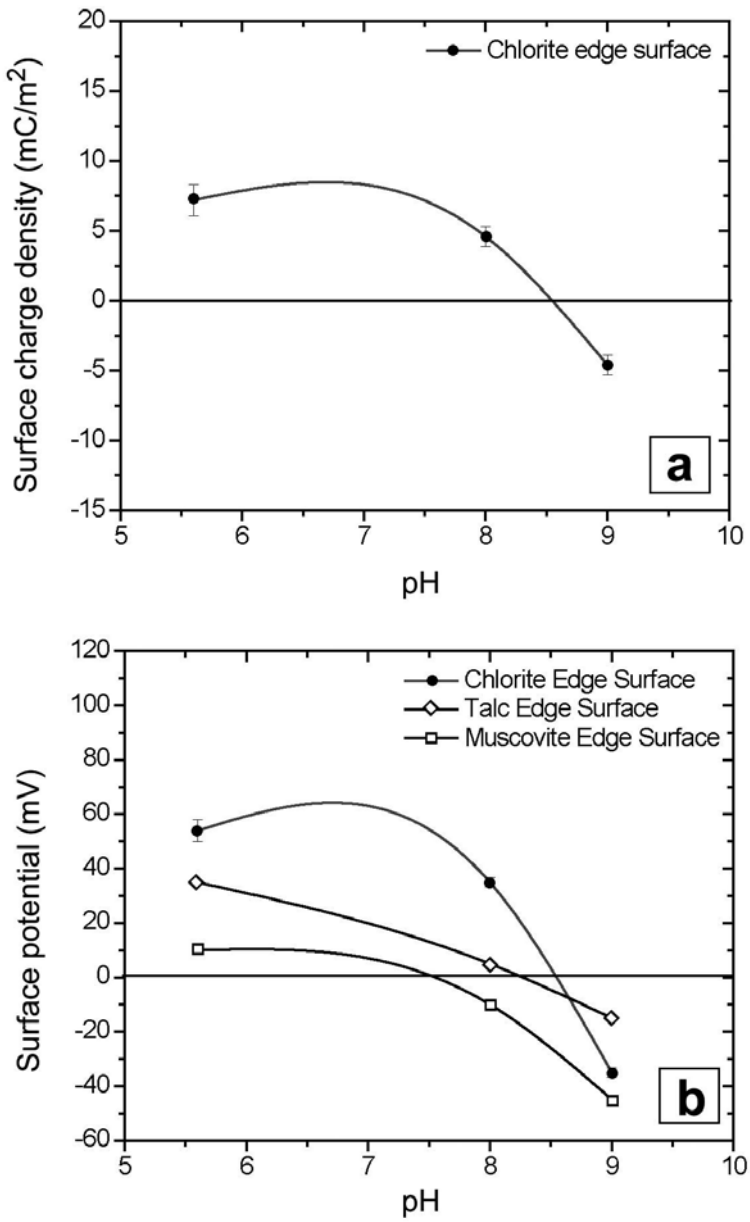


Figure 9. Surface charge density (a) and surface potential (b) of the chlorite edge surface as a function of pH. The error bars denote the standard deviation of multiple surface force measurements. The experimental results (plot with solid circle) are compared with the surface potentials of talc and muscovite edge surfaces from the literature (plot with open circle and open square) (Yan *et al.*, 2011).

https://doi.org/10.1346/CCMN.2013.0610212 Published online by Cambridge University Press

2011) (Figure 9b). Note that the IEP of the chlorite edge surface (~pH 8.5) is greater than the IEP of muscovite edge surface (~pH 7.5) and close to the IEP of talc edge surface (~pH 8.1). The charges at the edge surface of phyllosilicates arise mainly from the protonation and deprotonation reactions of the broken bonds of the surface groups. The general reaction formula is given as:

$$A^x + H^+ = AH^{x+1}$$

where $A^x$ represents a functional group with a charge of $x$ and $AH^{x+1}$ is the protonated form. Based on a Multi-Site Complexation model (MUSIC), the proton affinity of different surface groups at both basal and edge surfaces of phyllosilicates were studied (Nagashima and Blum, 1999; Avena *et al.*, 2003). The intrinsic protonation constants, $K_H$, of surface functional groups were calculated to describe the proton affinity (Table 1). Those authors found that the protonation constant for the siloxane group is very small ($\log K_H \sim -6.9$), suggesting that the siloxane structure is difficult to protonate. On the contrary, the surface functional groups at edge surfaces are much more reactive and can be protonated in the normal pH range. The groups of $Mg\text{-}OH^{2/3-}$ and $Al\text{-}OH^{1/2-}$ were found to be the dominant charging groups at phyllosilicate edge surfaces and can be protonated and become positively charged through the following reactions:

$$MgOH^{-2/3} + H^+ = MgOH_2^{+1/3}$$
$$AlOH^{-1/2} + H^+ = AlOH_2^{+1/2}$$

The fact that the protonation constant for $Mg\text{-}OH^{2/3-}$ is greater than for $Al\text{-}OH^{1/2-}$ (Table 1) indicates that $Mg\text{-}OH^{2/3-}$ is easier to protonate (Avena *et al.*, 2003; Tournassat *et al.*, 2004) and also explains why brucite has a larger IEP than gibbsite. As the edge surfaces of muscovite and talc contain the $Al\text{-}OH^{1/2-}$ groups and $Mg\text{-}OH^{2/3-}$ groups, respectively, the talc edge surface should have a larger IEP than the muscovite edge surface. This theoretical analysis has been confirmed by the experimental AFM results from the literature (Yan *et al.*, 2011).

In the case of the chlorite edge surface, $Mg\text{-}OH^{2/3-}$ is the main charging functional group, although a small amount of $Al\text{-}OH^{1/2-}$ is present in the brucite-like sheet. Theoretically, the ratio of Mg to Al in the chlorite octahedral sheet (both mica-like layer and brucite-like sheet) is 5:1. Instead of interlayer cations, chlorite has an additional brucite-like sheet between two mica-like layers, leading to a larger amount of $Mg\text{-}OH^{2/3-}$. Based on the crystal structure information, the ratio of the amount of $Mg\text{-}OH^{2/3-}$ in talc to that in chlorite is 3:4. Therefore, the chlorite edge surface is expected to be more positively charged at a given pH.

Chlorite can float with both cationic collectors (alkyl amines, alkyl ether amines, and quaternary ammonium salts) and anionic collectors (alkyl phosphonic acids, oleic acids, and xanthate) (Silvester *et al.*, 2011). Although the results from electrophoresis measurement cannot fully explain these flotation results, the establishment of the anisotropic surface charging of chlorite may help to explain the observed flotation results. In a study on the flotation of chlorite as a single mineral system, chlorite was found to be floated using lauryl amine with the greatest extent of recovery (~50%) at between pH 7 and pH 9 (Zheng *et al.*, 2009). Chlorite can also be floated using oleic acid. The recovery of chlorite at pH 8 with oleic acid is similar to that for lauryl amine (~50%), suggesting that both the cationic collector and anionic collector can adsorb at the chlorite surface at pH 8. According to the results of this study, the chlorite mica-like basal plane surface is negatively charged at pH 8, whereas the brucite-like basal surface and the edge surface are positively charged. Therefore, under these conditions the adsorption of the lauryl amine could occur at the mica-like surface and the oleic acid could adsorb at the brucite-like basal plane surface and at the edge surface, leading to flotation by either cationic or anionic surfactants (collectors), as observed experimentally. Clearly, the fundamental information on anisotropic surface-charge characteristics of chlorite derived from this study will permit design of more effective flotation reagent systems for chlorite-containing mineral systems.

Table 1. The protonation constants ($\log K_H$) of the surface groups in phyllosilicates (Yan *et al.*, 2011; Avena *et al.*, 2003; Tournassat *et al.*, 2004).

| Surface group | Location | Log $K_H^{int}$ |
|---|---|---|
| $Al_2$–OH | Basal surface | −1.5 |
| $Al_2$–$O^{1-}$ | Basal surface | 12.3 |
| $Si_2$-O | Basal surface | −16.9 |
| SiAl–$O^x$ | Edge surface | −16.9 to 12.3 |
| Si–OH | Edge surface | −1.9 |
| Si–$O^{1-}$ | Edge surface | 11.9 |
| Al–$OH^{1/2-}$ | Edge surface | 7.9 to 9.9 |
| Mg–$OH^{2/3-}$ | Edge surface | 10.0 |
| Si–O–Al–OH | Edge surface | 7.2 to 7.7 |
| Si–O–Mg–OH | Edge surface | 9.8 |

https://doi.org/10.1346/CCMN.2013.0610212 Published online by Cambridge University Press

## SUMMARY

The surface-charge properties of chlorite, which is a mixed-layer phyllosilicate, were characterized by measuring the surface forces between a silicon nitride tip and the chlorite surfaces using AFM. The mica-like face and brucite-like face of chlorite were prepared by splitting a chlorite crystal along its natural cleavage plane (001). Moreover, the chlorite edge surface was created using the ultramicrotome cutting technique. Both the basal-plane surface and the edge surface have a surface roughness of <1 nm, which should satisfy the requirement for AFM surface-force measurements.

The surface-force measurements were conducted in 1 mM KCl at pH 5.6, 8.0, and 9.0. The measured surface forces were fitted with the theoretical DLVO model. The surface potential and surface-charge density for chlorite basal-plane surfaces and edge surfaces were then determined from the fitting curve. A significant difference in charging behavior was observed for the chlorite mica-like face and the brucite-like face. At all three pH conditions, the chlorite mica-like face was negatively charged with the IEP <pH 5.6. In contrast, the chlorite brucite-like face is positively charged in this pH range and the IEP was >pH 9.0.

Surface charging of the chlorite edge surface was also examined. The transition from positive charge to negative charge was observed between pH 8.0 and pH 9.0. From the curve fitting, the IEP of the chlorite edge surface was estimated to be pH 8.5. This value was slightly greater than the IEP for muscovite and close to the IEP of talc-edge surfaces, which may be due to the greater number of magnesium hydroxide groups at the chlorite edge. Note that the term chlorite represents a group of minerals and contains many types of minerals which have the same structure but different chemical compositions. Therefore, different surface characteristics for different types of chlorite minerals can be expected and the values of the surface-charge density and surface potential obtained here may not be applicable to all of the minerals in the chlorite group.

The anisotropic surface characteristics of chlorite were also demonstrated. The surface-charging behavior of the chlorite basal plane surfaces and the edge surface was established as a function of pH. The results from the present research further established a better understanding of the charging behavior for phyllosilicates. The results are expected to provide a fundamental foundation for solving flotation issues, including collector adsorption, slime coating, and particle interactions.

## ACKNOWLEDGMENTS

Financial support for XY, JL, and JDM from the Division of Chemical Sciences, Geosciences and Biosciences, Office of Basic Energy Sciences, of the U.S. Department of Energy through Grant Number DE-FG03-93ER14315 is gratefully acknowledged. The authors express their appreciation to the Alberta Center for Surface Engineering and Science (ACSES) for their help with the XPS measurements and support for LY and ZX from the Natural Sciences and Engineering Research Council of Canada (NSERC) under the industry research chair program in Oil Sands Engineering.

## REFERENCES

Alvarez-Silva, M., Uribe-Salas, A., Mirnezami, M., and Finch, J. A. (2010) The point of zero charge of phyllosilicate minerals using the Mular–Roberts titration technique. *Minerals Engineering.* **23**, 383–389.

Assemi, S., Nalaskowski, J., Miller, J. D., and Johnson, W.P. (2006) Isoelectric Point of Fluorite by Direct Force Measurements Using Atomic Force Microscopy. *Langmuir.* **22**, 1403–1405.

Avena, M.J., Mariscal, M.M., and De Pauli, C.P. (2003) Proton binding at clay surfaces in water. *Applied Clay Science.* **24**, 3–9.

Butt, H.J., Graf, K., and Kappl, M. (2003) *Physics and Chemistry of Interfaces*. Wiley-VCH, Weinheim, Germany.

Deer, W.A., Howie, R.A., and Zussman, J. (1997) Rock Forming Minerals. *2nd ed.; The Geological Society*: London, Vol. 2B.

Drelich, J., Long, J., and Yeung, A. (2007) Determining Surface Potential of the Bitumen-Water Interface at Nanoscale Resolution using Atomic Force Microscopy. *The Canadian Journal of Chemical Engineering.* **85**, 625–634.

Drelich, J. and Wang, Y.U. (2011) Charge heterogeneity of surfaces: Mapping and effects on surface forces. *Advances in Colloid and Interface Science*, **160**, 91–101

Fornasiero, D. and Ralston, J. (2005) Cu(II) and Ni(II) activation in the flotation of quartz, lizardite and chlorite. *International Journal of Mineral Processing*, **76**, 75–81.

Fuerstenau, M.C., Jameson, G., and Yoon, R.H. (2007) *Froth flotation: A Century of Innovation*. Society for Mining Extraction and Exploration, Colorado, USA.

Fuerstenau, D.W. and Pradip (2005) Zeta potentials in the flotation of oxide and silicate minerals. *Advances in Colloid and Interface Science*, **114–115**, 9–26.

Gupta, V. and Miller, J.D. (2010) Surface force measurements at the basal planes of ordered kaolinite particles. *Journal of Colloid and Interface Science*, **344**, 362–371.

Gupta, V., Hampton, M.A., Stokes, J.R., Nguyen, A.V., and Miller, J.D. (2011) Particle interactions in kaolinite suspension and corresponding aggregate structures. *Journal of Colloid and Interface Science*, **359**, 95–103.

Harvey, C.C. and Murray, H.H. (1997) Industrial clays in the 21st century: A perspective of exploration, technology and utilization. *Applied Clay Science*, **11**, 285–310.

Isrealachvili, J.N. (1985) *Intermolecular and Surface Forces*. Academic Press, New York.

Leroy, P., Tournassat, C., and Bizi, M. (2011) Influence of surface conductivity on the apparent zeta potential of $TiO_2$ nanoparticles. *Journal of Colloid and Interface Science*, **356**, 442–453.

Long, J., Li, H., Xu, Z., and Masliyah, J.H. (2006) Role of colloidal interactions in oil sand tailings treatment. *AIChE Journal*, **52**, 371–383.

Mular, A.L. and Roberts, R.B. (1966) A simplified method to determine the isoelectric point of oxides. *Transactions of the Canadian Institute of Mining and Metallurgy*, **69**, 438–439.

Murray, H.H. (1991) Overview – clay mineral applications. *Applied Clay Science*, **5**, 379–395.

Murray, H.H. (2000) Traditional and new applications for kaolin, smectite, and palygorskite: a general overview. *Applied Clay Science*, **17**, 207–221.

Murray, H.H. and Kogel, J.E. (2005) Engineered clay products for the paper industry. *Applied Clay Science*, **29**, 199–206.

Nagashima, K. and Blum, F.D. (1999) Proton adsorption onto alumina: extension of multisite complexation (MUSIC) Theory. *Journal of Colloid and Interface Science*, **217**, 28–36.

Nalaskowski, J., Drelich, J., Hupka, J., and Miller, J.D. (2003) Adhesion between hydrocarbon particles and silica surfaces with different degrees of hydration as determined by the AFM colloidal probe technique. *Langmuir*, **19**, 5311–5317.

Nalaskowski, J., Abdul, B., Du, H., and Miller, J.D. (2007) Anisotropic character of talc surfaces as revealed by streaming potential measurements, atomic force microscopy, molecular dynamics simulations and contact angle measurements. *Canadian Metallurgical Quarterly*, **46**, 227–236.

Pokrovsky, O.S. and Schott, J. (2004) Experimental study of brucite dissolution and precipitation in aqueous solutions: surface speciation and chemical affinity control. *Geochimica et Cosmochimica Acta*, **68**, 31–45.

Silvester, E.J., Bruckard, W.J., and Woodcock, J.T. (2011) Surface and chemical properties of chlorite in relation to its flotation and depression. *Mineral Processing and Extractive Metallurgy*, **120**, 65–70.

Sondi, I. and Pravdić, V. (1996) Electrokinetics of natural and mechanically modified ripidolite and beidellite clays. *Journal of Colloid and Interface Science*, **181**, 463–469.

Sondi, I., Bišćan, J., and Pravdić, V. (1996) Electrokinetics of pure clay minerals revisited. *Journal of Colloid and Interface Science*, **178**, 514–522.

Sondi, I., Milat, O., and Pravdić, V. (1997) Electrokinetic potentials of clay surfaces modified by polymers. *Journal of Colloid and Interface Science*, **189**, 66–73.

Tournassat, C., Ferrage, E., Poinsignon, C., and Charlet, L. (2004) The titration of clay minerals II. Structure-based model and implications for clay reactivity. *Journal of Colloid and Interface Science*, **273**, 234–246.

Veeramasuneni, S., Yalamanchili, M.R., and Miller, J.D. (1996) Measurement of interaction forces between silica and α-alumina by atomic force microscopy. *Journal of Colloid and Interface Science*, **184**, 594–600.

Vincent, M.-M. and Jean Marc, D. (2007) Immersion of solids. *Encyclopedia of Surface and Colloid Science, Second Edition*, Taylor & Francis, pp. 2892–2905.

Vrdoljak, G.A., Henderson, G.S., Fawcett, J.J., Wicks, F.J., and Frederick, J. (1994) Structural relaxation of the chlorite surface imaged by the atomic microscope. *American Mineralogist*, **79**, 107–112.

Wallqvist, V., Claesson, P.M., Swerin, A., Schoelkopf, J., and Gane, P.A.C. (2006) Interaction forces between talc and hydrophobic particles probed by AFM. *Colloids and Surfaces A: Physicochemical and Engineering Aspects*, **277**, 183–190.

Wypych, F. and Satyanarayana, K.G. (2004) *Clay Surfaces: Fundamentals and Applications.* Academic Press, New York.

Yan, L., Englert, A.H., Masliyah, J.H., and Xu, Z. (2011) Determination of anisotropic surface characteristics of different phyllosilicates by direct force measurements. *Langmuir*, **27**, 12996–13007.

Yin, X. and Drelich, J. (2008) Surface charge microscopy: Novel technique for mapping charge-mosaic surfaces in electrolyte solutions. *Langmuir*, **24**, 8013–8020.

Zhang, J., Yoon, R.-H., and Eriksson, J.C. (2007) AFM surface force measurements conducted with silica in CnTACl solutions: Effect of chain length on hydrophobic force. *Colloids and Surfaces A: Physicochemical and Engineering Aspects*, **300**, 335–345.

Zhao, H., Bhattacharjee, S., Chow, R., Wallace, D., Masliyah, J.H., and Xu, Z. (2008) Probing surface charge potentials of clay basal planes and edges by direct force measurements. *Langmuir*, **24**, 12899–12910.

Zheng, G., Liu, L., Liu, J., Wang, Y., and Cao, Y. (2009) Study of chlorite and its influencing factors. *Procedia Earth and Planetary Science*, **1**, 830–837.

(*Received 11 September 2012; revised 15 March 2013; Ms. 712; AE: A. Thompson*)